PAPER

Check for updates

Selective hydrogenolysis of 5-hydroxymethylfurfural to 2,5-dimethylfuran with high yield over bimetallic Ru–Co/AC catalysts†

Zhen Dong, Yahui Zhang and Haian Xia [ID] *

Catalytic hydrogenolysis of 5-hydroxymethylfurfural (HMF) to 2,5-dimethylfuran (DMF) has become a hot topic in the bioenergy field in recent years. It remains a challenge to mediate the activation/hydrogenation/hydrogenolysis of C–O and C=O bonds of HMF at high temperatures. Herein, bimetallic Ru–Co/AC catalysts were prepared by the "two-step" reduction method and were used to catalyze the hydrogenolysis of HMF to DMF. The effects of different reduction methods, Ru/Co ratios, and Ru loading on the catalytic performances of the Ru–Co/AC catalysts were investigated, and the physicochemical properties of the catalysts were characterized by TEM, XPS, H_2-TPR, *etc.* It was found that the catalysts reduced by the "two-step" reduction method exhibited better catalytic activities than those fabricated by a single H_2 or $NaBH_4$ reduction method. The introduction of Co metals promoted the dispersion of Ru nanoparticles (NPs) on AC and the transfer of electrons from Co to Ru, thereby improving the catalytic activity. An excellent yield of DMF up to 97.9% and 98.7% conversion of HMF were achieved in a short time (1.5 h) under the optimal conditions (200 °C, 1 MPa). Furthermore, the possible reaction pathway for the hydrogenolysis of HMF to DMF over 5%Ru–1%Co/AC catalyst is also discussed. The work shows that the Ru–Co/AC catalysts have great potentials for the conversion of HMF into liquid fuel DMF.

1. Introduction

The demand for energy is growing rapidly with fast economic development. However, traditional fossil fuels have limited reserves and pose a potential threat to the sustainable development of human society because of environmental pollution by their combustion.[1–3] The high-value utilization of biomass has attracted much interest due to its abundant reserves, renewability, and low price.[4] Biomass has been used to produce liquid biofuels and high-value chemicals to mitigate environmental pollution, address the energy crisis, and promote sustainable development of human society.[5] Therefore, it is very critical to develop biomass energy as an alternative to conventional fossil energy sources.

HMF can be produced by dehydration of sugars and cellulose[6–8] and has been regarded as one of the top ten bio-platform compounds.[9] HMF can be used to synthesize levulinic acid, 2,5-dimethylfuran, 2,5-furan dicarboxylic acid, and other compounds through hydrogenation, oxidation, and other processes.[10] DMF, one of the hydrogenolysis products from HMF, has received much attention due to its advantages of

high-octane values (high explosion resistance), high energy densities, and low water solubility.[1,11] However, HMF possesses various functional groups including C=O, C–O, C=C bonds, and furan ring,[12,13] which could result in numerous intermediate products and very complex pathways in the hydrogenolysis of HMF. The most common products are summarized in Scheme 1. The dominant pathways are divided into two main ways according to the sequence of hydrogenation of the C=O bond and the hydrogenolysis of the C–O bond.[14] The first pathway involves the formation of DHMF through hydrogenation of the C=O bond followed by two continuous steps of hydrogenolysis of the C–O bonds. The second pathway involves the hydrogenolysis of the C–O bond before the hydrogenation of the C=O bond.[15] Both of these pathways involve the same reaction intermediate 5-methyl-2-furanmethanol which possesses a C–O bond, thus the activation of the C–O bond is a key step to increase the yield of DMF.

Up to now, the mono- and bi-metallic catalysts have been applied to the hydrogenolysis of HMF to DMF and satisfactory yields have been obtained,[16–18] and the typical catalysts and their catalytic properties are summarized in Table 1. Noble metal-based catalysts have received extensive attraction for their high catalytic activity and high product selectivity under mild conditions.[13,19] Priecel *et al.* used 5 wt% Ru/AC to obtain 96.5% HMF conversion with 83.5% yield of DMF at 150 °C, for 1 h.[20] David *et al.* developed Pd-based catalysts (Pd/Fe_2O_3) by the co-precipitation method and obtained a 72% yield of DMF at

Jiangsu Provincial Key Lab for the Chemistry and Utilization of Agro-forest Biomass, College of Chemical Engineering, Nanjing Forestry University, Nanjing, China. E-mail: haxia@njfu.edu.cn; Tel: +86-25-85427635
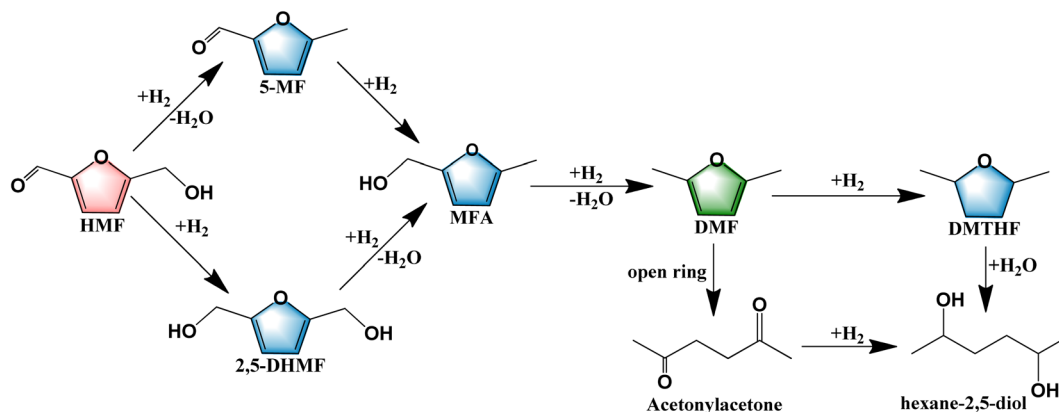
Scheme 1 Reaction pathways of the hydrogenolysis of HMF to DMF.

180 °C and 2.5 MPa.[21] The hydrogenation of the furan ring is easier than the C=O bonds over Pd metal sites owing to the narrow d-band of Pd metal and the different bonding modes, resulting in the generation of ring-opening by-products, which is adverse for obtaining a greater selectivity of DMF.[22] Non-noble metal-based catalysts have also gained significant interest due to their low cost.[23] Yang et al. fabricated Ni-based bimetallic catalysts (Ni–Co/C) using a wet impregnation method and achieved 99% conversion of HMF and 90% yield of DMF using formic acid as the hydrogen source at 210 °C for 24 h.[24] Zhang et al. used a co-precipitation method to prepare Cu/Al$_2$O$_3$ catalysts, which afforded a full conversion of HMF with a 73.9% yield of DMF by using formic acid as the hydrogen source at 240 °C for 6 h, attributed to a small Cu particle size and its strong acidic sites.[25]

To efficiently hydrogenolyze HMF to DMF, it is crucial to selectively hydrogenate/hydrogenolyze the C=O and C–O bonds and to avoid the over-hydrogenation or opening of the furan ring.[26] Previous research has shown that monometallic catalysts, especially noble-metal based catalysts, prefer the C–C hydrogenation to C–O bonds,[27] thereby resulting in over-hydrogenation. In order to obtain a high yield of DMF, one feasible strategy is to control the activation/hydrogenation/hydrogenolysis of C–O and C=C bonds on the metal NPs and

tune their electronic/geometric properties by introducing the second metal into a monometallic catalyst.[28] Furthermore, the acidity of catalysts has been reported to be another important factor for the hydrogenolysis of HMF to DMF because the acid sites profoundly affect the hydrogenolysis of the C–O bond.[29] Therefore, the introduction of the second metal with reasonable acidity into monometallic catalysts is a promising strategy to high-effectively hydrogenolyze HMF to DMF.

Ru-based catalysts are one of the most popular noble metal-based catalysts because of their excellent catalytic activities in many hydrogenation/hydrogenolysis reactions.[30] Generally, Ru metal has high selectivity for hydrogenation of the C=O bond due to its wide d-band,[31] which could be favorable for the transformation of HMF to DMF. However, monometallic Ru catalysts have a strong hydrogenation activity and are prone to excessive hydrogenation or opening of the furan ring of DMF.[32] For instance, 5%Ru/C was found to afford over-hydrogenation products of HMF, DMTHF and DHMTHF, with selectivities of 6.7% and 10.1%, respectively, and 5%Ru–10%MoO$_x$/C was found to afford DMTHF and DHMTHF with selectivities of 3.4% and 0.4%, respectively,[15] which proved that bimetallic catalysts can effectively reduce the excessive hydrogenation. Zu et al. used Ru/Co$_3$O$_4$ to obtain a 93.4% yield of DMF at relatively mild conditions for 24 h and prospected that CoO$_x$ acts as the

Table 1 Some typical catalysts and their catalytic performances for HMF to DMF reaction

Catalyst	Temp. (°C)	Pressure of H$_2$ (MPa)	Time (h)	Yield of DMF (%)	Ref.
Ru/C	200	2	2	94.7	39
Ru/NaY	220	1.5	1	78.0	47
Ru/RuO$_2$/C	190	—	6	72.0	58
Ru/Co$_3$O$_4$	130	0.7	24	93.4	59
Ru-MoO$_x$/C	180	1.5	1	79.8	15
Ru/CoFe-LDO	180	2	6	98.2	60
Pt-FeO$_x$/AC	180	1.5	6	91.1	61
Pd/Fe$_2$O$_3$	180	—	7.5	72.0	21
Co$_3$O$_4$	170	1	12	83.3	41
Ni–Mn/AC	180	2	4	98.5	55
Ni–Co/C	210	—	24	90.0	24
Ru–Co/AC	200	1	1.5	97.9	This work

adsorption metal sites of hydrogenation products and then breaks the C–O bond.[33] Wang *et al.* synthesized CuCo/CeO$_x$ by a co-precipitation method for catalytic transfer hydrogenation (CTH) of HMF to DMF, and a 95.4% yield of DMF was obtained at 170 °C, and proposed that CuCo bimetallic NPs promoted the cleavage of C–O of DHMF to produce DMF.[34] Therefore, it can be prospected that the introduction of Co metal could effectively break the C–O bond and enhance the selectivity of DMF. It is useful to introduce the second metal to enhance the selectivity of DMF.

It is widely accepted that zero-valent noble metal species are responsible for the dissociation of H$_2$ and serve as the hydrogenation active sites. Chemical reagents and gas reduction are common reduction methods to prepare hydrogenated catalysts.[35] Chemical reduction usually involves many reducers such as NaBH$_4$,[36] hydrazine hydrate,[37] and ethylene glycol, *etc.* For example, NaBH$_4$ reduction was employed to prepare Ru-based catalysts, which afford excellent catalytic activities due to RuO$_x$ being reduced completely and small Ru NPs sizes.[38] Gas reduction, such as H$_2$ reduction, can reduce metal oxides into various valence states and alloy catalysts at high temperatures, but high temperatures readily lead to the clustering of small NPs size into larger inactive metal NPs, especially for noble metal catalysts. Low-temperature chemical reduction can give very small metal NP sizes, but it is difficult to reduce transition metal oxides, such as CoO$_x$, and form active alloy sites which are very crucial for some synergetic catalytic reactions in some cases. Therefore, the combined use of both reduction methods is key to prepare catalysts with excellent catalytic properties through controlling small metal NPs sizes and the formation of alloy sites for synergetic catalysis.

As mentioned above, numerous promising catalysts for the hydrogenolysis of HMF to DMF have been reported, but low reaction temperatures and long reaction times (>12 h) are required in order to obtain high DMF yield and selectivity. So, novel catalysts with high selectivity at high temperatures for the hydrogenolysis of HMF to produce DMF in a short time are still to be explored. Herein, Ru–Co/AC bimetallic catalysts were prepared by a simple wet impregnation method, and Ru and Co metals were cascade reduced by NaBH$_4$ and H$_2$ gas reduction. The effect of different reaction conditions on the hydrogenolysis of HMF to DMF was studied. In addition, the nature of the catalyst was characterized by XRD, TEM, TPR, XPS, *etc.* The synergistic effect between Ru and Co species was elucidated and the deactivation reason of the catalysts was explained.

2. Experimental

2.1 Catalyst preparation

The bimetallic Ru–Co/AC catalysts were synthesized by the wet impregnation method. A typical prepared procedure of the Ru–Co/AC catalyst was described as follows. First, an appropriate amount of activated carbon (AC, S_{BET} = 1693.5 m^2 g^{-1}, Table S1†) was added into ultra-pure water, and then the desired mass of RuCl$_3$·xH$_2$O was dissolved into 0.2 mol L^{-1} HCl solution. Subsequently, the RuCl$_3$ solution was drop by drop added to the aqueous-AC mixed solution with stirring by a constant-flow

pump, and then the mixture was stirred for 12 h. Next, the 0.1 mol L^{-1} NaBH$_4$ solution was added dropwise to the impregnation Ru/AC solution in an ice water bath under vigorous stirring. After stirring for 4 h at room temperature, the mixture was filtered and washed with ultra-pure water. The second step is to incorporate Co onto the AC as follows, desired amounts of Co (NO$_3$)$_2$·6H$_2$O were dissolved into ultra-pure water and then added to the Ru/AC suspension solution. After 12 hours, the mixture was filtered, washed, and dried at 60 °C for 12 hours. Finally, the catalyst precursor was calcined in a flow of 5.0 vol.%H$_2$/N$_2$ flow at 300 °C for 2 h. Similarly, the Ru–Re/AC and Ru–Mo/AC catalysts were prepared through the wet impregnation method, only Co (NO$_3$)$_2$·6H$_2$O was replaced by NH$_4$ReO$_4$ and (NH$_4$)$_6$Mo$_7$O$_{24}$·4H$_2$O, respectively. For comparison, the monometallic Ru/AC or Co/AC were also fabricated by a similar method. The resulting bimetallic catalysts were denoted as x%Ru–y%M/AC (M = Co, Re, and Mo), where x and y refer to the corresponding metal loadings. The elemental contents of the catalysts analyzed by ICP-AES are listed in Table S2.† As can be seen, the final Ru and Co loadings of the as-prepared catalysts roughly match the Ru and Co precursor contents.

2.2 Catalytic performances

The catalytic performances were evaluated by a stainless-steel high-pressure autoclave (50 mL) equipped with mechanical stirring. The catalyst (25 mg), HMF (1.25 wt% relative to THF), and THF (20 mL) were added to the autoclave and then it was sealed followed by flushing with N$_2$ and H$_2$ three times respectively to remove air. Then, the autoclave was pressurized with a desired H$_2$, heated to the target temperature reacted at the set time. The reaction products were analyzed by a Shimadzu LC-2050 equipped with a UV detector. A mobile phase was composed of 60% methanol and 40% pure water at a flow rate of 1 mL min^{-1}, and a C$_{18}$ column was used for product separation with UV wavelengths of 284 nm (HMF) and 219 nm (DMF). HMF and DMF were quantified based on the external standard method. The conversion of HMF and yield and selectivity of DMF was calculated using the following equations:

$$\text{HMF conversion (\%)} = \left\{ 1 - \frac{\text{Mole of HMF}}{\text{Initial mole of HMF}} \right\} 100\%$$

$$\text{DMF yield (\%)} = \left\{ \frac{\text{Mole of DMF}}{\text{Initial mole of HMF}} \right\} 100\%$$

$$\text{DMF selectivity (\%)} = \left\{ \frac{\text{Yield of DMF}}{\text{Conversion of HMF}} \right\} 100\%$$

2.3 Catalysts characterization

X-ray diffraction patterns (XRD) were obtained with a Rigaku Ultima IV X-ray diffractometer (Rigaku, Matsubara Cho, Japan) equipped with a Cu Kα X-ray source operating at 40 kV and 30

mA. X-ray photoelectron spectra (XPS) were recorded on a KRATOS AXIS Ultra DLD instrument (Shimadzu, Tokyo, Japan). Transmission electron microscope (TEM) image was carried out with a JEM-200CX transmission electron microscope (JEOL, Tokyo, Japan). Elemental analysis was performed with an icpmsPE300D inductively coupled plasma atomic emission spectrometer (ICP-AES). The specific surface area was measured by N_2 isothermal adsorption on BSD-PM2. The samples were outgassed at 120 °C for 5 h before analysis. Temperature programmed reduction (TPR) was undertaken on BELCAT-A equipped with a TCD detector to measure the reduction behaviors of the catalysts. For H_2-TPR experiments, the 50 mg sample was heated to 800 °C at the rate of 10 °C min^{-1}, after being cooled to room temperature, 5 vol.% H_2/N_2 gas was used as the reduced gas. Temperature programmed desorption of NH_3 (NH_3-TPD) was conducted on BELCAT-A to analyze the amount of acid sites of the catalysts. 50 mg sample was purged by He at 400 °C before adsorption, then cooled to 100 °C to saturate with NH_3 and swept by He to remove the physically adsorbed NH_3 for 0.5 h, and then the samples were heated to 400 °C at the rate of 10 °C min^{-1}.

3. Results and discussion

3.1 The nature of the catalysts

3.1.1 XRD analysis. The XRD patterns of the support AC, monometallic Ru/AC, Co/AC, and bimetallic Ru–Co/AC catalysts are shown in Fig. 1. All catalysts have a broad peak at around 24° and 43.7°, which is attributed to the (002) and (101) crystal planes of AC,[39] respectively. After the introduction of metal, no diffraction peaks associated with Ru or Co metal NPs were observed for the catalysts, which indicates that these particles were highly dispersed on the surface of the AC with small particle sizes.[40]

3.1.2 TEM images. Fig. 2 shows the TEM images of different catalysts and the diameter of particles. The average size of the Ru particles for the 5%Ru/AC catalyst was about 6.70 nm (Fig. 2a). The large particle size of the catalyst may be due to the agglomeration of Ru NPs on the AC surface during reduction (Fig. 2b). As shown in Fig. 2c, the mean particle size of 1%Co/AC is small due to the low loading of Co and its uniform distribution. Compared to the 5%Ru/AC catalyst, the average particle size of 5%Ru–1%Co/AC catalyst shown in Fig. 2d is about 2.43 nm which indicates that the addition of Co species successfully promotes the dispersion of Ru particles on AC, resulting in a decrease in the particle size of the catalyst. A lattice spacing of 0.20 nm is also observed (Fig. 2d), indicating the presence of the CoO (200) facet or the Co metal (111) facet.[41] In other words, the oxidation state of Co (Co^{2+}) and the zero-valence state of Co (Co^0) co-existed in the 5%Ru–1%Co/AC
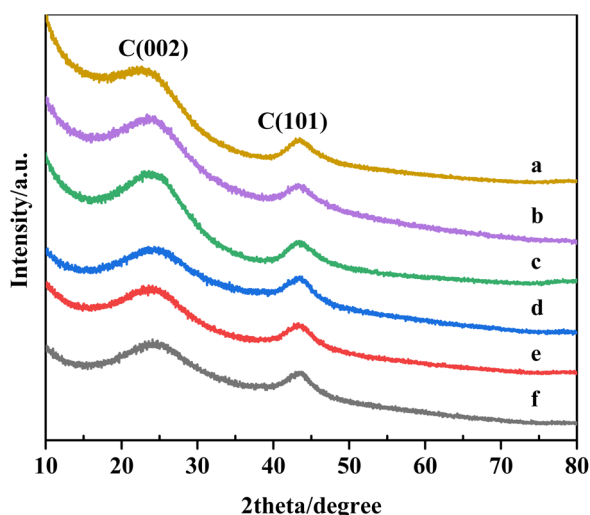

Fig. 1 XRD patterns of (a) AC, (b) 5%Ru–5%Co/AC, (c) 5%Ru–0.5%Co/AC, (d) 5%Ru–1%Co/AC, (e) 1%Co/AC, and (f) 5%Ru/AC.
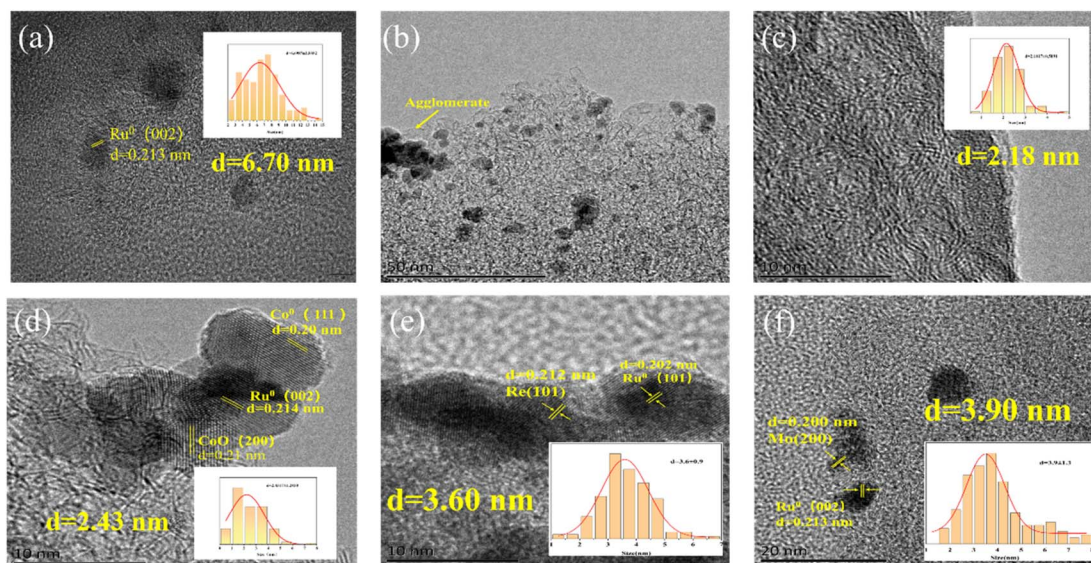

Fig. 2 TEM images of (a, b) 5%Ru/AC catalyst, (c) 1%Co/AC, (d) 5%Ru–1%Co/AC, (e) 5%Ru–1% Re/AC, and (f) 5%Ru–1%Mo/AC.

Table 2 The effect of the reduction methods on the hydrogenolysis of HMF to DMF[a]

Entry	Catalyst	Conv. (%)	Yield (%)	Sel. (%)
1[b]	5%Ru–1%Co/AC	98.7	97.9	99.2
2[c]	5%Ru–1%Co/AC-C-300	74.0	52.6	71.2
3[d]	5%Ru–1%Co/AC-C-NaBH$_4$	98.5	89.7	91.1
4[e]	5%Ru–1%Co/AC-400	98.6	92.9	94.2
5[f]	5%Ru–1%Co/AC-200	98	93.4	94.7

[a] Reaction conditions: catalyst, 25 mg, HMF, 1.25 wt% relative to THF; THF, 20 mL. 200 °C, 1 MPa, 1.5 h. [b] Ru was reduced by NaBH$_4$ and Co was reduced at 300 °C for 2 h. [c] Ru and Co were reduced by H$_2$ at 300 °C for 2 h. [d] Ru and Co were reduced by NaBH$_4$. [e] Ru was reduced by NaBH$_4$ and Co was reduced at 400 °C for 2 h. [f] Ru was reduced by NaBH$_4$ and Co was reduced at 200 °C for 2 h.

catalyst. Moreover, an intimate contact between Ru NPs and Co NPs is also observed, which suggests that the synergistic effects could take place in the conversion of HMF or even form Ru–Co alloy (Fig. 2d and S2 of ESI†). This also explains why the bimetallic catalysts have superior catalytic properties than the monometallic catalysts (Table 2). In general, CoO$_x$ is considered as Lewis acid site, which could facilitate the activation of the C–O group.

To explore the reason for the better catalytic performance of 5%Ru–1%Co/AC than that of 5%Ru–1%Re/AC and 5%Ru–1%Mo/AC, we also characterized 5%Ru–1%Re/AC and 5%Ru–1%Mo/AC by TEM. As shown in Fig. 2e and f, the average particle sizes of 5%Ru–1%Re/AC and 5%Ru–1%Mo/AC are about 3.60 and 3.90 nm respectively, which is slightly larger than that of 5%Ru–1%Co/AC. We can also observe the slight agglomeration of Ru NPs on 5%Ru–1%Re/AC and 5%Ru–1%Mo/AC (Fig. S2h and 2i), which shows that the dispersion of particles on 5%Ru–1%Re/AC and 5%Ru–1%Mo/AC is inferior than that on 5%Ru–1%Co/AC. According to the results above, we speculate that the reason that the Ru NPs particle size of 5%Ru–1%Co/AC is smaller and has higher dispersion compared to the other catalysts. In other words, the interactions between Ru and Co species could be stronger.

3.1.3 XPS analysis. To confirm the interaction between Ru and Co species, the surface chemical states of 5%Ru/AC, 1%Co/AC, and 5%Ru–1%Co/AC catalysts were characterized using XPS. Because the photoemission line of Ru 3d overlapped with the line of C 1s, the Ru 3p spectra were employed for analyzing the surface species. As shown in Fig. 3a, for the 5% Ru/AC catalyst, the binding energy of 462.9 and 485.3 eV was attributed to Ru^0 3p$_{1/2}$ and Ru^0 3p$_{3/2}$, respectively.[5] In addition, the peaks of Ru^{n+} are not observed in Fig. 3a, indicating that Ru^{3+} was completely reduced, which is consistent with the TEM result. In contrast to the 5%Ru–1%Co/AC catalyst, the binding energy of Ru over the 5%Ru/AC catalyst shifted to a higher binding energy, which suggests that the electron transfer from Co to Ru could occur[42](Fig. 3a and c). Meanwhile, the chemical status of Co 2p was measured by XPS, and the results are shown in Fig. 3b and d, for the 1%Co/AC catalyst, the binding energies of 781.0, and 783.1 eV were attributed to Co^{3+} 2p$_{3/2}$, and Co^{2+} 2p$_{3/2}$. The binding energies of 786.4 and 804.8 eV were
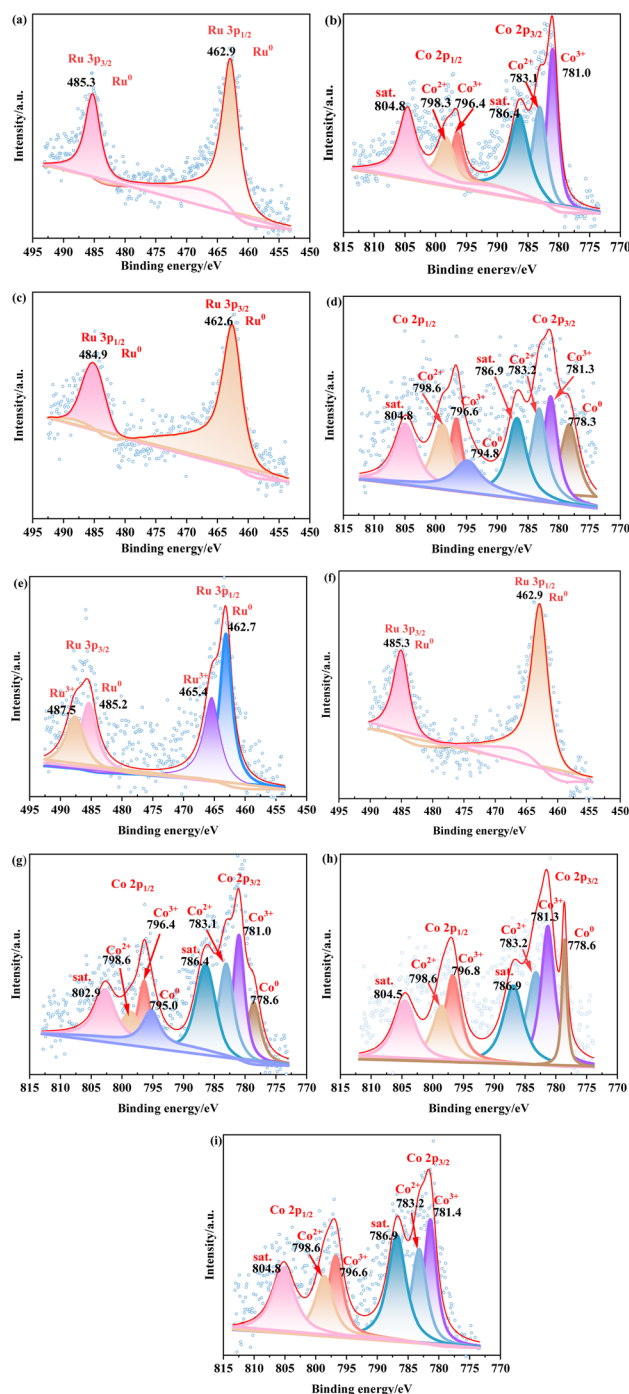

Fig. 3 (a) Ru 3p XPS of 5%Ru/AC, (b) Co 2p XPS of 1%Co/AC, (c) Ru 3p XPS of 5%Ru–1%Co/AC-300, (d) Co 2p XPS of 5%Ru–1%Co/AC-300, (e) Ru 3p XPS of 5%Ru–1%Co/AC-C-300, (f) Ru 3p XPS of 5%Ru–1%Co/AC-C-NaBH$_4$, (g) Co 2p XPS of 5%Ru–1%Co/AC-C-NaBH$_4$, (h) Co 2p XPS of 5%Ru–1%Co/AC-400, (i) Co 2p XPS of 5%Ru–1%Co/AC-200.

attributed to Co 2p$_{3/2}$ and Co 2p$_{1/2}$ satellite peaks, respectively.[43,44] As observed in Fig. 3d, the binding energy of Co species of the 5%Ru–1%Co/AC catalyst was upshifted compared to the 1%Co/AC catalyst, which was explained by the electron transfer from Co to Ru. However, in Fig. 3d, a definite Co metal

peak appears with a binding energy of 778.3 eV, indicating that some Co^{2+} was reduced into Co metal.[43] Both 1%Co/AC and 5% Ru–1%Co/AC were reduced at 300 °C, however, the Co 2p XPS of 5%Ru–1%Co/AC contained a peak related to Co^0 metal. The results indicate that the presence of Ru enhances the reduction of the Co species, which is also confirmed by this work.[45] This phenomenon can be explained by the adsorption of H_2 on Ru and then dissociation into highly reactive hydrogen atoms, the H_2 spillover contributed to the reduction of CoO_x when Ru and Co atoms were close on AC.[46]

As shown in Fig. 3e, for the 5%Ru–1%Co/AC-C-300 catalyst (Ru and Co were reduced by H_2 at 300 °C for 2 h), the peaks of Ru^0 and Ru^{n+} are observed, indicating that Ru^{3+} was incompletely reduced and the oxidation state of Ru (Ru^{n+}) and the zero-valence state of Ru (Ru^0) co-existed in the 5%Ru–1%Co/AC-C-300 catalyst, resulting in insufficient of active hydrogenation sites on the catalyst. As shown in Fig. 3f and g, for the 5%Ru–1% Co/AC-C-NaBH$_4$ catalyst (Ru and Co were reduced by NaBH$_4$), the binding energies of Ru and Co species of the 5%Ru–1%Co/ AC C–NaBH$_4$ catalyst were not shifted obviously compared to the 5%Ru/AC and 1%Co/AC catalysts, indicating that there is little or no electron transfer between Ru and Co species and the synergistic effect between Ru and Co species is extremely weak. As illustrated in Fig. 3h and i, for the 5%Ru–1%Co/AC-400 catalyst (Ru was reduced by NaBH$_4$ and Co was reduced at 400 °C for 2 h), a larger Co metal peak appears with a binding energy of 778.3 eV, which can be explained by the fact that more Co^{2+} was reduced into Co metal at 400 °C. For the 5%Ru–1%Co/ AC-200 catalyst (Ru was reduced by NaBH$_4$ and Co was reduced at 200 °C for 2 h), no obvious Co metal peak appears because Co^{2+} is hard to be reduced to Co metal at this reduction temperature.

3.1.4 H$_2$-TPR and NH$_3$-TPD analysis. Temperature-Programmed Reduction (TPR) was used to measure the reduction behaviors of the catalysts, as illustrated in Fig. 4a. For the 5% Ru/AC catalyst, the reduction peak at 125 °C was attributed to the weak interaction between Ru and AC, and the reduction

peak at 250 °C was related to the reduction of RuO_x species which strongly interacted with AC.[47,48] The reduction peak at about 540 °C could be associated with the formation of hydrocarbons from the reduction of the AC catalyzed by the Ru species and the decomposition of the catalyst.[49] For the 1%Co/ AC catalyst, two reduction peaks appeared at about 460 °C and 600 °C, respectively. The peaks at 460 °C and 600 °C were attributed to the reduction of Co^{3+} to Co^{2+}, and Co^{2+} into Co^0, respectively.[50,51] For the 5%Ru–1%Co/AC catalyst, the peak at 100 °C was related to RuO_x to Ru^0. We speculate that the peak at around 260 °C could be the overlapping reduction peaks from RuO_x to Ru^0 and Co^{3+} to Co^{2+}.[33,52] However, the reduction peak of Co^{2+} to Co^0 located at 550 °C, was lower than the 1%Co/AC catalyst (600 °C), which could be explained by the presence of Ru promotes the reduction of the Co species.[45] These results suggest that there exists a synergistic effect between Ru and Co species, which is consistent with the XPS results.

The acid sites of the catalysts were analyzed by NH$_3$-TPD, as shown in Fig. 4b. Almost no peak was observed over the 5%Ru/ AC catalyst, indicating that the monometallic catalyst almost had no acidity. And for the 1%Co/AC catalyst, there was an obvious peak at 280 °C, indicating that the catalyst possesses medium acidic sites.[53] After the incorporation of Co species, a peak at about 280 °C was observed over the 5%Ru–1%Co/AC catalyst, which showed that the addition of Co species endows the acidic sites of the bimetallic catalyst.

3.2 Hydrogenolysis of HMF to DMF

3.2.1 Effect of the reduction methods. Table 2 demonstrates the effect of reduction methods on the catalytic activity of catalysts. The low conversion of HMF and the inferior yield of DMF were obtained when using 5%Ru–1%Co/AC-C-300 catalyst reduced at 300 °C. This is due to the incomplete reduction of the Ru^{3+} causing the insufficient of active hydrogenation sites on the catalyst surface according to the XPS results. When the catalysts were only reduced with NaBH$_4$, the yield of DMF was
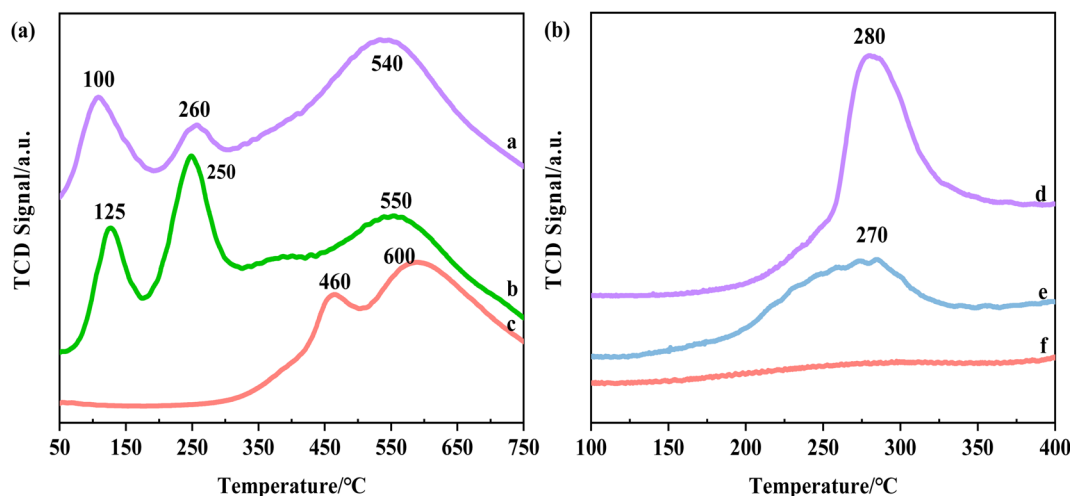

Fig. 4 The H$_2$-TPR profile of (a) 5%Ru–1%Co/AC, (b) 5%Ru/AC, (c) 1%Co/AC and TheNH$_3$-TPD profile of (d) 1%Co/AC, (e) 5%Ru–1%Co/AC, (f) 5% Ru/AC.

89.7%, lower than that of 5%Ru–1%Co/AC reduced with NaBH$_4$ and H$_2$ (Table 2, entries 1 and 3). Based on the XPS results, a possible explanation is that there is little or no electron transfer between Ru and Co species and the synergistic effect between Ru and Co species is extremely weak. Finally, we investigated the effect of the reduction temperature on the catalytic ability. When the catalysts were reduced at 200 °C and 400 °C, the distribution between the active hydrogenation sites and acidic sites on the catalyst surface were not optimal, resulting in the relatively low yield of DMF of 93.4% and 92.9%, respectively, which were lower than the 97.9% yield of DMF over the 5%Ru–1%Co/AC catalyst. Therefore, we determined that the optimal reduction temperature for Co on 5%Ru–1%Co/AC catalyst is 300 °C.

3.2.2 Selection of the second metal in Ru-based bimetallic catalysts. Here, Re, Mo, and Co metals were selected as the second metals to introduce the Ru/AC catalyst (Table 3, entries 4–6). It is also worth noting that for the initial second metal screening, 50 mg catalyst and 20 mL THF solution of HMF (2.5 wt%) were used. However, we found that 20 mL of THF solution of HMF (1.25 wt%) and 25 mg catalyst was found to obtain better results (Table S3†). When compared to the Ru/AC catalyst, the addition of transition metals to the catalysts increased both the conversion of HMF and the yield of DMF. Among them, 5%Ru–1%Co/AC catalyst has the highest yield of DMF, meaning that Co is more favorable than Mo and Re in the hydrogenolysis of HMF due to the stronger synergistic effects between Ru and Co species. Therefore, Co was selected as the second metal to fabricate a bimetallic catalyst with Ru.

Meanwhile, we prepared 5%Ru/AC and 1%Co/AC catalysts to compare their catalytic performances, as shown in Table 3. It can be seen that the 5%Ru–1%Co/AC catalyst outperformed both the monometallic 5%Ru/AC and 1%Co/AC catalysts in the hydrogenolysis of HMF. It is worth noting that some ring-opening products of DMF were detected over 5%Ru/AC by GC-MS (Fig. S2†), which verifies that the monometallic Ru catalysts are prone to excessive hydrogenation or ring-opening reactions. To confirm the synergistic effect between Ru and Co species, we physically mixed 5%Ru/AC and 1%Co/AC and then used them for the hydrogenolysis of HMF (Table 3, entry 3), and found that the yield of DMF was much lower than that of 5%Ru–1%Co/AC. This suggests that the synergistic effect

Table 3 The effects of different metals on the hydrogenolysis of HMF to DMF

Entry	Catalyst	Conv. (%)	Yield (%)	Sel. (%)
1[a]	5%Ru/AC	93.8	74.5	79.4
2[a]	1%Co/AC	42.2	21.3	50.4
3[a]	5%Ru/AC + 1%Co/AC	95.7	81.3	85.0
4[b]	5%Ru–1%Co/AC	99.3	85.9	86.6
5[b]	5%Ru–1%Re/AC	99.3	82.6	83.2
6[b]	5%Ru–1%Mo/AC	99.3	81.3	81.9

[a] Reaction conditions: catalyst, 25 mg; HMF, 1.25 wt% relative to THF; THF, 20 mL. 200 °C, 1 MPa, 1.5 h. [b] Reaction conditions: catalyst, 50 mg; HMF, 2.5 wt% relative to THF; THF, 20 mL. 200 °C, 1 MPa, 1.5 h.

Table 4 The effect of Ru/Co ratios on the hydrogenolysis of HMF to DMF[a]

Entry	Catalyst	Conv. (%)	Yield (%)	Sel. (%)
1	2.5%Ru–1%Co/AC	83.0	70.6	85.1
2	5%Ru–0.5%Co/AC	98.6	96.7	98.0
3	5%Ru–1%Co/AC	98.7	97.9	99.2
4	5%Ru–5%Co/AC	98.7	95.8	97.1

[a] Reaction conditions: catalyst, 25 mg, HMF, 1.25 wt% relative to THF; THF, 20 mL. 200 °C, 1 MPa, 1.5 h.

between Ru and Co species enhanced the catalytic activity of the 5%Ru–1%Co/AC catalyst.

3.2.3 Effect of Ru/Co ratios. Table 4 shows the effect of different Ru/Co ratios on the catalytic activity of catalysts. The low conversion of HMF and yield of DMF was obtained over 2.5%Ru–1%Co/AC. As Ru loading was raised to 5%, 5%Ru–1% Co/AC displayed better catalytic activity (Table 4, entries 1, and 3). The increased Ru loading significantly enhanced the catalytic activity, resulting in a more than 27% increase in the yield of DMF. When the Ru loading was kept constant at 5% and changing Co contents, the yield of DMF increased gradually as the Co loading was increased to 1%, but it decreased when the Co loading was further increased to 5% (Table 4, entries 2, 3 and 4), indicating that there were too many acidic sites and an increase in the ring-opening reactions of the HMF.

3.2.4 Effects of various reaction conditions. Fig. 5 summarizes the results of the hydrogenolysis of HMF to DMF over 5%Ru–1%Co/AC catalyst under different reaction conditions. As the reaction temperature increased from 180 °C to 200 °C, both the conversion of HMF and the yield of DMF increased. The inferior activity of 5%Ru–1%Co/AC catalyst for the hydrogenolysis of HMF at low temperature may be attributed to a substantial quantity of hydrogenation intermediates of HMF, such as 5-MF and MFA. However, when the reaction temperature was raised to 220 °C, the yield of DMF reduced substantially. Previous work has shown that acidic metal oxides, like CoO$_x$, might efficiently break the C–O bond.[54] However, further increasing temperature, deep hydrogenation, or even ring opening of the furan ring could take place. Therefore, it seems that the optimal temperature for the reaction is 200 °C.

At a lower pressure of 0.5 MPa, the hydrogenolysis of HMF was incomplete, producing numerous intermediates, and resulting in a low yield of DMF. When H$_2$ pressure was increased to 1 MPa, a 97.9% yield of DMF was achieved, which could be explained by the increase of H$_2$ pressure promoting the dissolution of H$_2$ in THF. When the pressure of H$_2$ was increased to 2 MPa, excessive H$_2$ pressure resulted in the production of by-products and a decrease in the yield of DMF.

Fig. 5c shows the influence of reaction time on the hydrogenolysis of HMF. As can be seen, 97.4% conversion of HMF and 76.0% yield of DMF were obtained within 0.5 hours. When the reaction time was extended to 1.5 hours, the conversion of HMF did not increase, but the enhancement in yield of DMF was more significant, perhaps because extending the time
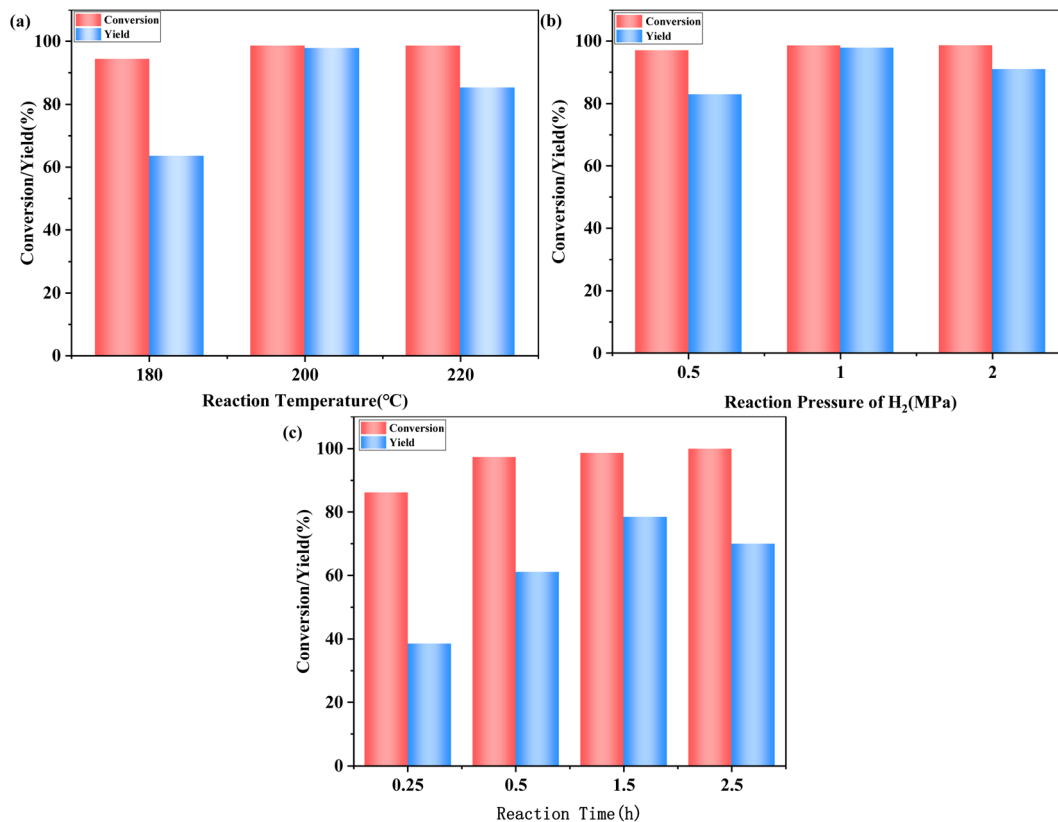
Fig. 5 Effects of (a) reaction temperature, (b) pressure of H_2, (c) reaction time.

further promoted the conversion of intermediates to DMF. When further extended to 2.5 hours, the yield of DMF decreased. This suggests that DMF may be converted into more undesirable by-products if excessive reaction time is employed.

3.2.5 The pathway for hydrogenolysis of HMF to DMF. To study the reaction pathway for the hydrogenolysis of HMF to DMF, a series of reactions were carried out at 200 °C under 1 MPa of H_2 for 5/15/30/90 min over 5%Ru–1%Co/AC, and then the reaction mixture was analyzed by GC and GC-MS. As can be seen from GC-MS (Fig. S1c†), in addition to the unreacted HMF and target product DMF, reaction intermediates 5-methyl-furfural (5-MF), 5-methylfurfuryl alcohol (MFA) were also detected, but 2,5-dihydroxymethylfurfural (DHMF) was not produced. As shown in Fig. S2,† the yield of DMF increased gradually within 90 min while HMF was almost fully converted after 30 min, and the yield of 5-MF decreased gradually within 90 min whereas the yield of MFA firstly increased before 15 min and then reduced until it was completely converted after 90 min. This result clearly demonstrates that 5-MF and MFA are the most intermediates in the hydrogenolysis of HMF.

Based on the above-mentioned results and the previously reported literature,[39,55–57] we speculate that the following reaction pathway for the hydrogenolysis of HMF to DMF over 5% Ru–1%Co/AC. Firstly, CoO_x species on the catalyst surface bound the oxygen atom of the C–O group in HMF, and the cleavage of the C–O bond occurred under the synergistic effects of Ru^0 and CoO_x species to form the 5-MF. Next, MFA was

formed from the hydrogenation of 5-MF by Ru NPs. Finally, the target product DMF was obtained from the hydrogenolysis of MFA *via* a similar reaction pathway as the hydrogenolysis of HMF to 5-MF.

3.2.6 The recyclability of the catalyst. The recyclability of catalysts is critical for the hydrogenolysis of HMF to DMF. In this work, the recyclability and stability of 5%Ru–1%Co/AC catalyst were evaluated. The 5%Ru–1%Co/AC catalyst was used for the hydrogenolysis of HMF to DMF under 1 MPa of H_2 at 200 °C for 1.5 h. To better understand the real recyclability of 5%Ru–1%Co/AC catalyst, a special reaction was carried out at 80 °C under 0.25 MPa of H_2 for 0.5 h to keep the conversion of HMF at about 50%. After the first run, the 5%Ru–1%Co/AC catalyst was separated through filtration from the reaction product, and washed 5 times with 10 mL of THF, dried at 80 °C for 12 h eventually. From Fig. 6a, more than 90% yield of DMF and 98% conversion of HMF can be obtained after three runs. From Fig. S5,† about 50% conversion of HMF can be kept before the fourth runs, but we failed to observe DMF due to the low reaction temperature. These results demonstrate that the 5% Ru–1%Co/AC catalyst was stable and efficient for the hydro-genolysis of HMF to DMF. Compared to the fresh catalyst, the average diameter of the recovered 5%Ru–1%Co/AC catalyst increased largely after four runs (Fig. 6b), which leads to a decrease in the conversion of HMF and yield of DMF. On the other hand, the leaching of Ru and Co metals (Table S2, entry
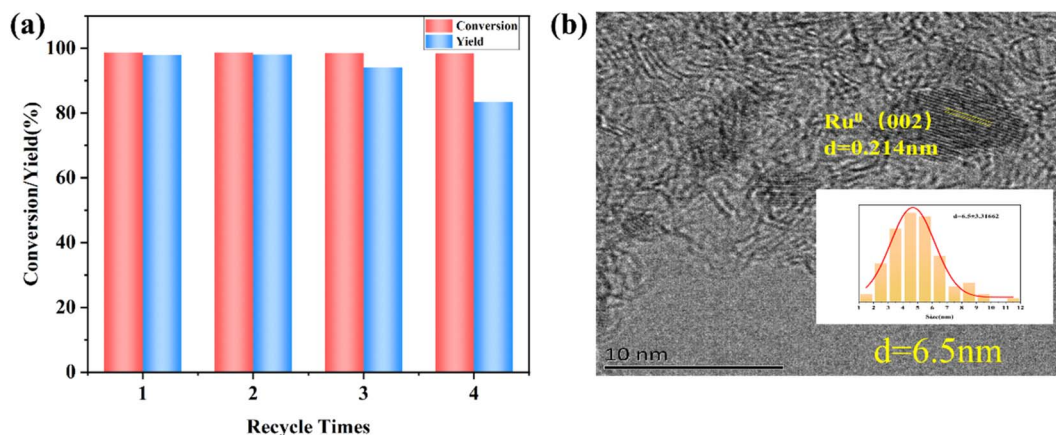
Fig. 6 (a) Recyclability and reusability of 5%Ru–1%Co/AC, and (c) TEM images of 5%Ru–1%Co/AC (after 4 runs).

6†) could be one of the deactivation reasons for the 5%Ru–1% Co/AC catalyst.

4. Conclusions

In this work, bi-functional Ru–Co/AC catalysts were prepared by the "two-step" reduction method, which can efficiently convert HMF to DMF. It was revealed that the introduction of Co species decreased the average particle size of Ru NPs, which promoted the catalytic hydrogenolysis of HMF of the Ru–Co/AC catalysts. In addition, it was found that the highest DMF yield of 5%Ru–1%Co/AC could be achieved by first reducing Ru by NaBH$_4$ followed by impregnating with Co, and finally reducing it by H$_2$. An excellent yield of up to DMF 97.9% with the HMF conversion of 98.7% was achieved in a short period (1.5 h). Ru NPs act as an active hydrogenation site and CoO$_x$ serves as the acid site to synergistically activate and crack the C–O bonds during the hydrogenolysis reaction of HMF. The synergistic effect between Ru and Co NPs improves the selective hydrogenolysis of HMF to DMF. Moreover, the catalyst has good recyclability and could be reused at least 3 times without a significant loss in activity, and the slight deactivation was attributed to the increase in particle sizes and the leaching of the active metal. This work demonstrates that the Ru–Co/AC catalysts have great potential for the high-efficiency transformation of bio-platform molecules to biofuels.

Author contributions

Zhen Dong: conceptualization, formal analysis, investigation, resources, writing original draft, visualization. Yahui Zhang: data summary and calibration. Haian Xia: writing review and editing, funding acquisition.

Conflicts of interest

The authors declare that they have no known competing financial interests or personal relationships that could have appeared to influence the work reported in this paper.

Acknowledgements

References

1 Y. Román-Leshkov, C. J. Barrett, Z. Y. Liu and J. A. Dumesic, *Nature*, 2007, **447**, 982–985.

2 C. G. Yoo and T. H. Kim, *Energies*, 2020, **13**, 5438.

3 H. L. Long, X. B. Li, H. Wang and J. D. Jia, *Renewable Sustainable Energy Rev.*, 2013, **26**, 344–352.

4 L. Hu, L. Lin, Z. Wu, S. Y. Zhou and S. J. Liu, *Renewable Sustainable Energy Rev.*, 2017, **74**, 230–257.

5 W. W. Zhu, H. M. Yang, J. Z. Chen, C. Chen, L. Guo, H. M. Gan, X. G. Zhao and Z. S. Hou, *Green Chem.*, 2014, **16**, 1534–1542.

6 R. Karinen, K. Vilonen and M. Niemelä, *ChemSusChem*, 2011, **4**, 1002–1016.

7 A. A. Rosatella, S. P. Simeonov, R. F. M. Frade and C. A. M. Afonso, *Green Chem.*, 2011, **13**, 754–793.

8 R.-J. van Putten, J. C. van der Waal, E. de Jong, C. B. Rasrendra, H. J. Heeres and J. G. de Vries, *Chem. Rev.*, 2013, **113**, 1499–1597.

9 G. Yong, Y. G. Zhang and J. Y. Ying, *Angew. Chem., Int. Ed.*, 2008, **47**, 9345–9348.

10 J.-P. Lange, W. D. van de Graaf and R. J. Haan, *ChemSusChem*, 2009, **2**, 437–441.

11 R. Insyani, D. Verma, S. M. Kim and J. Kim, *Green Chem.*, 2017, **19**, 2482–2490.

12 H. Wang, C. Zhu, D. Li, Q. Liu, J. Tan, C. Wang, C. Cai and L. Ma, *Renewable Sustainable Energy Rev.*, 2019, **103**, 227–247.

13 Y. Sun, J. Zheng, J. Xu, K. Yang, Z. Zhu, T. Su, H. Ge, W. Ren and H. Lü, *Fuel*, 2022, **315**, 123226.

14 H. Son Le, Z. Said, M. Tuan Pham, T. Hieu Le, I. Veza, V. Nhanh Nguyen, B. Deepanraj and L. Huong Nguyen, *Fuel*, 2022, **324**, 124474.

15 Y. Yang, Q. Y. Liu, D. Li, J. Tan, Q. Zhang, C. G. Wang and L. L. Ma, *RSC Adv.*, 2017, **7**, 16311–16318.

16 D. S. Brands, E. K. Poels and A. Bliek, *Appl. Catal., A*, 1999, **184**, 279–289.

17 Y. Takeda, Y. Nakagawa and K. Tomishige, *Catal. Sci. Technol.*, 2012, **2**, 2221–2223.

18 J. Zhang, L. Lin and S. Liu, *Energy Fuels*, 2012, **26**, 4560–4567.

19 W. T. Lu, J. C. Chen, J. Feng and J. Yu, *Rare Met. Mater. Eng.*, 2012, **41**, 184–188.

20 P. Priecel, N. A. Endot, P. D. Carà and J. A. Lopez-Sanchez, *Ind. Eng. Chem. Res.*, 2018, **57**, 1991–2002.

21 D. Scholz, C. Aellig and I. Hermans, *ChemSusChem*, 2014, **7**, 268–275.

22 S. Sitthisa and D. E. Resasco, *Catal. Lett.*, 2011, **141**, 784–791.

23 X. C. Zheng, X. Y. Wang, L. H. Yu, S. R. Wang and S. H. Wu, *Progr. Chem.*, 2006, **18**, 159–167.

24 P. P. Yang, Q. N. Xia, X. H. Liu and Y. Q. Wang, *Fuel*, 2017, **187**, 159–166.

25 Z. H. Zhang, C. X. Wang, X. Gou, H. Chen, K. Q. Chen, X. Y. Lu, P. K. Ouyang and J. Fu, *Appl. Catal., A*, 2019, **570**, 245–250.

26 G. H. Wang, J. Hilgert, F. H. Richter, F. Wang, H. J. Bongard, B. Spliethoff, C. Weidenthaler and F. Schüth, *Nat. Mater.*, 2014, **13**, 294–301.

27 Q. Wang, S. Santos, C. A. Urbina-Blanco, W. Zhou, Y. Yang, M. Marinova, S. Heyte, T.-R. Joelle, O. Ersen, W. Baaziz, O. V. Safonova, M. Saeys and V. V. Ordomsky, *Appl. Catal., B*, 2022, **300**, 120730.

28 Y. Y. Li, R. N. Wang, B. W. Huang, L. L. Zhang, X. R. Ma, S. K. Zhang, Z. G. Zhu, H. Y. Lü and K. X. Yang, *Appl. Surf. Sci.*, 2022, **604**, 154579.

29 J. Kuljiraseth, A. Wangriya, J. M. C. Malones, W. Klysubun and S. Jitkarnka, *Appl. Catal., B*, 2019, **243**, 415–427.

30 M. Chidambaram and A. T. Bell, *Green Chem.*, 2010, **12**, 1253–1262.

31 T. W. H. AN, *Chem. Ind. Eng. Prog.*, 2021, **40**, 824–834.

32 M. Luneau, J. S. Lim, D. A. Patel, E. C. H. Sykes, C. M. Friend and P. Sautet, *Chem. Rev.*, 2020, **120**, 12834–12872.

33 Y. Zu, P. Yang, J. Wang, X. Liu, J. Ren, G. Lu and Y. Wang, *Appl. Catal., B*, 2014, **146**, 244–248.

34 X. F. Wang, C. C. Zhang, Z. Y. Zhang and Q. B. Li, *Fuel*, 2022, **320**, 123996.

35 A. W. Heinen, J. A. Peters and H. van Bekkum, *ChemInform*, 2001, **328**, 449–457.

36 T. Furusawa, M. Shirasu, K. Sugiyama, T. Sato, N. Itoh and N. Suzuki, *Ind. Eng. Chem. Res.*, 2016, **55**, 12742–12749.

37 F. T. Jere, J. E. Jackson and D. J. Miller, *Ind. Eng. Chem. Res.*, 2004, **43**, 3297–3303.

38 T. Shi, Degree Thesis of Master, Zhejiang University of Technology, 2016.

39 L. Hu, X. Tang, J. X. Xu, Z. Wu, L. Lin and S. J. Liu, *Ind. Eng. Chem. Res.*, 2014, **53**, 3056–3064.

40 L. Y. Song, X. H. Li, H. N. Wang, H. H. Wu and P. Wu, *Catal. Lett.*, 2009, **133**, 63–69.

41 D. Li, Q. Y. Liu, C. H. Zhu, H. Y. Wang, C. H. Cui, C. G. Wang and L. L. Ma, *J. Energy Chem.*, 2019, **30**, 34–41.

42 Z. Gao, G. L. Fan, M. R. Liu, L. Yang and F. Li, *Appl. Catal., B*, 2018, **237**, 649–659.

43 F. B. Noronha, M. Schmal, B. Moraweck, P. Delichère, M. Brun, F. Villain and R. Fréty, *J. Phys. Chem. B*, 2000, **104**, 5478–5485.

44 M. Esen, S. Akmaz, S. N. Koc and M. A. Gürkaynak, *J. Sol-Gel Sci. Technol.*, 2019, **91**, 664–672.

45 C. E. Scott, P. Betancourt, M. J. Pérez Zurita, C. Bolívar and J. Goldwasser, *Appl. Catal., A*, 2000, **197**, 23–29.

46 W. Wang, N. Li, S. S. Li, G. Y. Li, F. Chen, X. R. Sheng, A. Q. Wang, X. D. Wang, Y. Cong and T. Zhang, *Green Chem.*, 2016, **18**, 1218–1223.

47 A. S. Nagpure, N. Lucas and S. V. Chilukuri, *ACS Sustainable Chem. Eng.*, 2015, **3**, 2909–2916.

48 S. Z. Zheng, X. Y. Cao, Q. Zhou, S. H. Wang, G. S. Hu, J. Q. Lu, M. F. Luo and Y. J. Wang, *J. Fluorine Chem.*, 2013, **145**, 132–135.

49 I. Rossetti, N. Pernicone and L. Forni, *Appl. Catal., A*, 2003, **248**, 97–103.

50 H.-Y. Lin and Y.-W. Chen, *Mater. Chem. Phys.*, 2004, **85**, 171–175.

51 S. R. de Miguel, M. C. Román-Martínez, E. L. Jablonski, J. L. G. Fierro, D. Cazorla-Amorós and O. A. Scelza, *J. Catal.*, 1999, **184**, 514–525.

52 J. Yu, D. Zhao, X. L. Xu, X. Wang and N. Zhang, *ChemCatChem*, 2012, **4**, 1122–1132.

53 Y. Chu, T. Zhang, J. Guo, C. Liu, H. Yin, X. Zhu and Y. Liu, *J. Rare Earths*, 2015, **33**, 371–381.

54 W. J. Xu, H. F. Wang, X. H. Liu, J. W. Ren, Y. Q. Wang and G. Z. Lu, *Chem. Commun.*, 2011, **47**, 3924–3926.

55 Y. X. Liu, X. Y. Shi, J. B. Hu, K. Liu, M. Zeng, Y. X. Hou and Z. J. Wei, *ChemSusChem*, 2022, **15**, e202200193.

56 T. Thananatthanachon and T. B. Rauchfuss, *Angew. Chem., Int. Ed.*, 2010, **49**, 6616–6618.

57 J. Jae, W. Q. Zheng, R. F. Lobo and D. G. Vlachos, *ChemSusChem*, 2013, **6**, 1158–1162.

58 P. Panagiotopoulou, N. Martin and D. G. Vlachos, *J. Mol. Catal. A: Chem.*, 2014, **392**, 223–228.

59 Y. H. Zu, P. P. Yang, J. J. Wang, X. H. Liu, J. W. Ren, G. Z. Lu and Y. Q. Wang, *Appl. Catal., B*, 2014, **146**, 244–248.

60 Q. Y. Li, P. Man, L. Q. Yuan, P. L. Zhang, Y. Li and S. Y. Ai, *Mol. Catal.*, 2017, **431**, 32–38.

61 Y. J. Xin, S. C. Li, H. Y. Wang, L. G. Chen, S. Li and Q. Y. Liu, *Catalysts*, 2021, **11**, 915.